Heliyon 5 (2019) e01815

Contents lists available at ScienceDirect

Heliyon

journal homepage: www.heliyon.com

Activation energy and dual stratification effects for Walter-B fluid flow in view of Cattaneo-Christov double diffusionon

Misbah Ijaz *, Muhammad Ayub

Department of Mathematics, Quaid-I-Azam University 45320, Islamabad, 44000, Pakistan

ARTICLE INFO

Keywords:
Mechanics
Thermodynamics
Nanomechanics
Heat transfer
Activation energy
Non-linear mixed convection
Heat generation/absorption
Cattaneo-Christov double-diffusion model
Walter-B nanofluid
Double stratification

ABSTRACT

The purpose of the present article is to explore the novel aspects of activation energy in nonlinearly convective flow of Walter-B nanofluid in view of Cattaneo-Christov double diffusion model over a permeable stretched sheet. Generalized forms of Fourier's and Fick's law are utilized through Cattaneo-Christov double diffusion. Walter-B nanomaterial model is used that describes the significant slip mechanism namely Brownian and thermophoresis diffusions. Double stratification, heat generation/absorption and chemical reaction are considered. Modified Arrhenius formula for activation energy is implemented. The acquired nonlinear system is cracked through homotopic analysis method. Effects of emanating variables are examined through graphs and tables. It is evident that temperature distribution and thermal boundary layer thickness is monotonically dwindling function of thermal stratification parameter (P_1), thermal relaxation time (δ_2) and upsurge for the thermophoresis parameter (N_t), heat generation/absorption parameter (B_1), Brownian motion parameter (N_b). Nanoparticle concentration is directly comparable to the activation energy of reaction and impact of thermal relaxation time is qualitatively opposite to that of thermophoretic force.

1. Introduction

In the eighteenth and early nineteenth centuries, scientists well-thought-out that all bodies contained an undetectable fluid which they named as "**caloric**". Caloric was assigned a variety of characteristics, some of which evinced to be inconsistent with nature (e.g., it had mass and it could not be produced/destroyed) but its most noteworthy feature was that it moves from hot bodies into colder ones. It was very favourable approach to visualize the concept of heat. Basically, heat transfer is the flow of thermal energy driven by thermal non-equilibrium. Heat flows continuously from our bloodstream to the air round us. The flow of heat is all-pervasive. The heat transfer has significance in manufacturing and industrial processes such as power generation, cooling of atomic reactors, energy production, paper production, cooling of electronic devices and numerous others. Some significant work can be viewed via refs. [1, 2, 3, 4]. Heat and mass transfer is generally analysed by employing renowned Fourier's law of heat theory [5] and Fick's law of mass diffusion [6]. The main paradox of Fourier model is that it yields to parabolic energy expression which spectacles that the whole system is instantly responded by the initial disturbance. Cattaneo [7] has overcome this inadequacy by adding thermal relaxation time in the classical Fourier's law which yields hyperbolic energy equation [8, 9]. Christov [10] proposed a frame-indifferent generalization of the Cattaneo model with thermal relaxation time in terms of Oldroyd's upper-convected derivatives acknowledged as Cattaneo-Christov heat flux model. Numerical analysis has been accomplished to explore the significant impacts of Cattaneo-Christov model heat flux for Maxwell liquid by Khan et al. [11]. Ijaz et al. [12] explored the impacts of Cattaneo-Christov double diffusion scheme for nonlinear convective and stratified flow of Maxwell nanofluid with binary chemical reaction and activation energy. Khan et al. [11] provided a numerical study to inspect Cattaneo-Christov heat flux for steady flow of Maxwell liquid due to an exponentially stretchable surface. Muhammad et al [13] developed the mathematical model for squeezing flow of viscous fluid with heat and mass fluxes using Cattaneo-Christov theory. Hayat et al. [14] also explored the effect of Cattaneo-Christov heat and mass flux for 3D incompressible flow of nanoliquid. Sui et al. [15] examined Maxwell nanofluid in view of Cattaneo-Christov double diffusion over a stretched surface. For more studies on Cattaneo-Christov double diffusion with different geometries, one may consult refs. [16, 17, 18].

Mass transport is a universal phenomenon in nature that is driven by solutal non-equilibrium state of medium or mixture. The heat and mass

* Corresponding author.
E-mail address: misbahijaz@math.qau.edu.pk (M. Ijaz).

https://doi.org/10.1016/j.heliyon.2019.e01815
Received 24 January 2019; Received in revised form 15 April 2019; Accepted 22 May 2019

transfer problems with binary chemical reaction has broad applications in chemical engineering, extrusion processes, geothermal reservoirs, nuclear reactor cooling and polymer industries. The heterogeneous species having different concentration level in a mixture move themselves from a region of greater concentration to lower ones. Ravindran et al. [19] examined chemical reaction, heat generation/absorption and combined effect of free and forced convection over a nonlinearly stretched surface. Nayak et al. [20] inspected the combined effects of chemical reaction and magnetic field on viscoelastic fluid over a stretching sheet embedded in a porous medium. Effects of MHD chemical reaction for convective flow are investigated over a rotating cone through porous medium by Mallikarjuna [21]. Hayat et al. [22] deliberated the unsteady flow with heat and mass transfer of a third grade fluid over a stretching surface in the presence of chemical reaction. Zubair et al. [23] discussed the stratified flow problem of ferromagnetic Powell-Eyring fluid with modified Fourier law of heat conduction over a stretched plate.

Stratification is a formation/deposition of layers in vertical direction that plays an innovative role in various industrial processes, engineering fields and in atmosphere. In real-world where heat and mass transfer run in parallel, it becomes essential to study the results of dual stratification on the nanofluids. Stratified fluids are bountiful in the environment, i.e., heat discharge into the atmosphere, storage systems for thermal energy like solar ponds, transfer of heat from thermal sources such as groundwater reservoirs and oceans and many identical examples. Thermal stratification improves the concentration level of oxygen in the lower bottom of see or reservoirs. Effect of duel stratification on mixed convective flow of Maxwell nanofluid in presence of heat generation/absorption is observed by Abbasi et al. [24]. Stratified flow of ferromagnetic nanofluid with nonuniform heat generation/absorption is scrutinized by Ijaz et al. [25]. Hayat et al. [26] explored the mixed convective flow of thixotropic nanofluid in presence of magnetic field and duel stratification over a linear stretched sheet. Impact of thermal and solutal stratification on convective flow of nanofluid by an inclined stretched sheet is discovered by Hayat et al. [27]. Some remarkable studies regarding stratification can be found via refs. [27, 28, 29].

Recent developments in nanoscience originate from the inspection of physical characteristics of material at nanoscale level. Among several industrial applications of nanosciences, nanofluids constitute an evolving field in heat transfer. Besides anomalously high thermal conductivity, nanofluids have superior stability that avoids quick settling and clogging near the boundaries of heat transfer devices. The impetus in nanofluid research stems from the heat transfer amplification in processes involving micro-manufacturing, microchips in computer processors, space cooling, fuel cells, nuclear engineering, hybrid-powered engines, diesel engine oil air-conditioners/refrigerators and many others. Buongiorno [30] established a two-phase model for inspecting thermal energy transport via nanofluids. In his innovative work, he deliberated the seven potential features of nanofluid comprise of particle agglomeration, inertia, nanoparticle size, Magnus effect, nanoparticle volume fraction, thermophoresis and Brownian motion. In all these mechanisms, thermophoresis and Brownian motion are very significant and fascinating. Later, Tiwari and Das [31] developed a simple model in which thermophysical properties were observed as functions of nanoparticle volume fraction. Both the above stated models have been effectively applied to address several diverse flow problems. Kuznetsov and Nield [32] used Buongiorno model to define the features of Brownian motion and thermophoretic diffusion on nanofluid flow embedded through a porous medium. Ijaz et al. [33] employed Buongiorno model for ferromagnetic Maxwell liquid with nonlinear thermal radiation, non-uniform heat source/sink and binary chemical reaction. Bhatti et al. [34] discussed thermo-diffusion and thermal radiation on Williamson nanofluid over a permeable sheet.

Viscoelastic fluid is a subclass of non-Newtonian fluids that exhibit both viscous and elastic characteristics. The significance of viscoelastic flow is increasing gradually in paper and petroleum industries, chemical technology and Geophysical fluid dynamics. Viscoelastic materials are used for isolating vibration, dampening noise, and absorbing shock. They give off the energy absorbed as heat. Sorbothane is recognized worldwide as the best viscoelastic material for absorbing shock, isolating vibration and damping noise. No synthetic rubber or polymer can dissipate energy as effectively. Sorbothane is a highly damped, viscoelastic polymeric solid that flows like a liquid under load. Since its introduction in 1982, Sorbothane has been used in many energy absorbing product applications. Our engineers partnered with NASA to design a unique Sorbothane isolator that protects the vital shuttle cameras during launch. Walters-B fluid model [35] with limiting viscosity at low shear rates and short memory coefficient is one of the best models to describe the characteristics of a viscoelastic fluid.

Keeping these in the view the purpose of present paper is to analyse the impacts of activation energy for nonlinearly convective flow of Walter-B nanofluid [36] over a permeable stretched surface. The novelty of the present problem is to study the Arrhenius activation energy phenomena for viscoelastic nanofluid model in view of heat generation/absorption, nonlinear mixed convection and duel stratification. The novel features of binary chemical reaction is analysed to characterize the impact of activation energy in presence of Cattaneo-Christov double-diffusion model. The obtained non-linear system of ordinary differential equations is tackled for series solutions through homotopic scheme [37, 38, 39]. The behaviour of several flow parameters on the physical quantities of interest are deliberated through graphs.

2. Model

Present study explores the novel features of activation energy for unsteady and nonlinear convective flow of Walter-B nanofluid in view of Cattaneo-Christov double-diffusion model. Non-uniform heat generation/absorption, dual stratification nonlinear mixed convection, chemical reaction and activation energy are considered. Thermal and concentration buoyancy forces are applied to the fluid with double stratification effect due to temperature and concentration variation. Walter-B fluid occupies the semi-infinite region $y > 0$ over the surface with stretching velocity $U_w(x)$ (see Fig. 1). Temperature and the nanoparticle fraction at surface of the sheet are T_w and C_w respectively. While the ambient temperature and nanoparticles volume fraction is specified by T_∞ and C_∞, respectively. Walter-B nanomaterial model is engaged which defines the important slip mechanism namely Brownian and thermophoresis diffusions. Under the above mentioned assumptions along with boundary layer approximations, the constitutive equations [36, 37, 38, 39] are presented in Eqs. (1) and (2)

$$\frac{\partial u}{\partial x}+\frac{\partial v}{\partial y}=0, \tag{1}$$

$$\left.\begin{aligned} u\frac{\partial u}{\partial x}+v\frac{\partial u}{\partial y}=\nu_1\frac{\partial^2 u}{\partial y^2}-\Lambda_1\left(u\frac{\partial^3 u}{\partial x\partial y^2}+v\frac{\partial^3 u}{\partial y^3}+\frac{\partial u}{\partial x}\frac{\partial^2 u}{\partial y^2}-\frac{\partial u}{\partial y}\frac{\partial^2 u}{\partial x\partial y}\right) \\ +\frac{\widehat{g}_2}{\rho_f}\left[\Gamma_1(T-T_\infty)+\Gamma_2(T-T_\infty)^2+\Gamma_3(C-C_\infty)+\Gamma_4(C-C_\infty)^2\right], \end{aligned}\right\} \tag{2}$$

Here, u and v defines the velocity components along x and y-axis respectively (Λ_1) for elastic parameter, $\left(\nu_1\left(=\frac{\mu}{\rho}\right)_f\right)$ for kinematic viscosity, (ρ_f) for fluid density (Γ_1, Γ_2, Γ_3, Γ_4) for thermal and solutal expansion coefficients depending on linear and nonlinear form, respectively. Cattaneo-Christov heat and mass fluxes [40] are expressed in Eqs. (3) and (4)

$$\vec{\mathbf{q}}+\widehat{\Gamma}_e\left[\frac{\partial\vec{\mathbf{q}}}{\partial t}+\vec{V}_1.\nabla\vec{\mathbf{q}}-\vec{\mathbf{q}}.\nabla\vec{V}_1+\left(\nabla.\vec{V}_1\right)\vec{\mathbf{q}}\right]=-k_f\nabla T, \tag{3}$$

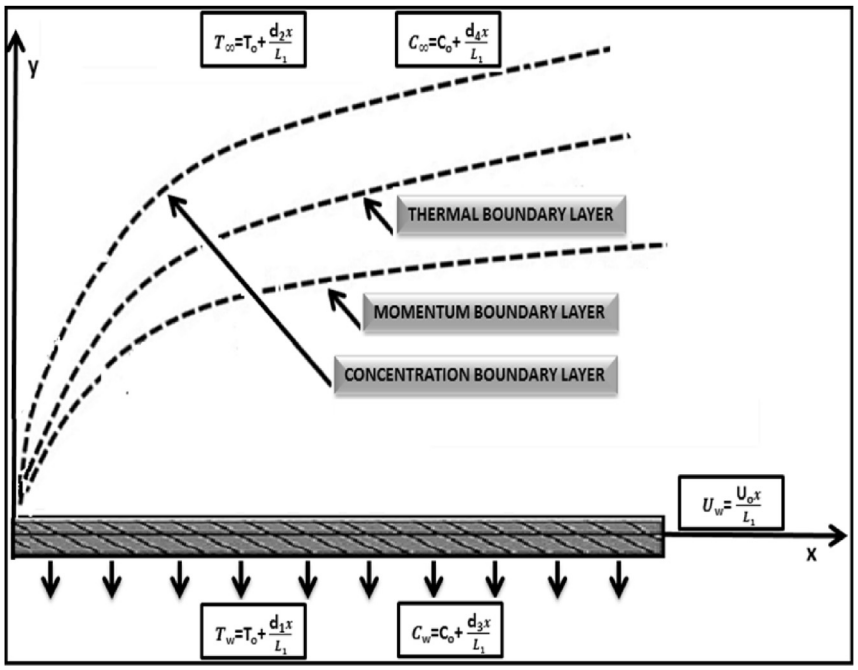

Fig. 1. Flow geometry.

$$\vec{j}+\hat{\Gamma}_c\left[\frac{\partial\vec{j}}{\partial t}+\vec{V}_1.\nabla\vec{j}-\vec{j}.\nabla\vec{V}_1+(\nabla.\vec{V}_1)\vec{j}\right]=-D_B\nabla C, \tag{4}$$

where $(\vec{q},\ \vec{j})$ symbolize for heat and mass fluxes, $(\hat{\Gamma}_e,\ \hat{\Gamma}_c)$ for relaxation time of heat and mass fluxes respectively, (k_f) the thermal conductivity, (D_B) the Brownian diffusivity and $(\vec{V}_1)$ the velocity vector. The above Eqs. (3) and (4) reduces to the classical Fourier's and Fick's law when $\hat{\Gamma}_e = \hat{\Gamma}_c = 0$. According to the conditions of steady and incompressible flow i.e., $\left(\frac{\partial\rho}{\partial t}=0\ and\ \nabla.\vec{V}_1=0\right)$, Eqs. (3) and (4) reduces to Eqs. (5) and (6)

$$\vec{q}+\hat{\Gamma}_e\left[\vec{V}_1.\nabla\vec{q}-\vec{q}.\nabla\vec{V}_1\right]=-k_f\nabla T, \tag{5}$$

$$\vec{j}+\hat{\Gamma}_c\left[\vec{V}_1.\nabla\vec{j}-\vec{j}.\nabla\vec{V}_1\right]=-D_B\nabla C, \tag{6}$$

Two-dimensional energy and concentration expressions are presented in Eqs. (7) and (8)

$$u\frac{\partial T}{\partial x}+v\frac{\partial T}{\partial y}+\hat{\Gamma}_e\Pi_e=\frac{k_f}{(\rho C_p)_f}\frac{\partial^2T}{\partial y^2}+\frac{\hat{Q}_m}{(\rho C_p)_f}+\tau_1 D_B\frac{\partial C}{\partial y}\frac{\partial T}{\partial y}+\frac{\tau_1 D_T}{T_\infty}\left(\frac{\partial T}{\partial y}\right)^2, \tag{7}$$

$$\left.\begin{aligned}&u\frac{\partial C}{\partial x}+v\frac{\partial C}{\partial y}+\hat{\Gamma}_c\Pi_c=D_B\frac{\partial^2C}{\partial y^2}+\frac{D_T}{T_\infty}\left(\frac{\partial^2T}{\partial y^2}\right)-\hat{k}_2(C-C_\infty)\\&-\hat{K}_r^2(C_w-C_o)\left(\frac{T}{T_\infty}\right)^n exp\left[-\frac{E_2^*}{Tk^*}\right],\end{aligned}\right\} \tag{8}$$

Cattaneo-Christove expressions (Eqs. (9) and (10)) are as follows

$$\Pi_e=u^2\frac{\partial^2T}{\partial x^2}+v^2\frac{\partial^2T}{\partial y^2}+\frac{\partial T}{\partial y}\left(u\frac{\partial v}{\partial x}+v\frac{\partial v}{\partial y}\right)+\frac{\partial T}{\partial x}\left(u\frac{\partial u}{\partial x}+v\frac{\partial u}{\partial y}\right)+2uv\frac{\partial^2T}{\partial y\partial x}, \tag{9}$$

$$\Pi_c=u^2\frac{\partial^2C}{\partial x^2}+v^2\frac{\partial^2C}{\partial y^2}+\frac{\partial C}{\partial y}\left(u\frac{\partial v}{\partial x}+v\frac{\partial v}{\partial y}\right)+\frac{\partial C}{\partial x}\left(u\frac{\partial u}{\partial x}+v\frac{\partial u}{\partial y}\right)+2uv\frac{\partial^2C}{\partial y\partial x}, \tag{10}$$

$$\left.\begin{aligned}&u(x,y)=\frac{U_ox}{L_1},\ v(x,y)=V_2,\ T=T_w=T_o+\frac{d_1x}{L_1},\ C=C_w=C_o+\frac{d_3x}{L_1}\ at\ y=0,\\&u\to0,\ v\to0,\ T\to T_\infty=T_o+\frac{d_2x}{L_1},\ C\to C_\infty=C_o+\frac{d_4x}{L_1}\ when\ y\to\infty,\end{aligned}\right\} \tag{11}$$

in the above expressions $\tau_1\left(=\frac{(\rho C_p)_p}{(\rho C_p)_f}\right)$ stands for specific heat ratio, (D_T) for themophoretic diffusion coefficient, (L_1) for reference length, (U_o) for reference velocity, $(-1<n<1)$ for fitted rate constants, $(\hat{k}_2)$ for chemical reaction parameter, (C) for concentration, $(\hat{K}_r^2)$ chemical reaction rate, (E_2^*) for activation energy, $k^*\ (=8.61\times10^{-5}eV/K)$ for the Boltzmann constant and $(V_2<0)$ uniform velocity of suction or injection $(V_2>0)$, respectively.

The non-uniform heat generation/absorption $\hat{Q}_m$ [41] is modeled in Eq. (12)

$$\hat{Q}_m=\frac{U_w(x)k_f}{x\nu_1}\left[B_1(T_w-T_o)\frac{\partial G}{\partial\Omega_1}+B_2(T-T_\infty)\right], \tag{12}$$

Here, $B_1>0$ and $B_2>0$ corresponds to heat generation case while $B_1<0$ and $B_2<0$ resembles to the heat absorption.

Introducing the following the self-similar transformations (Eq. 13)

$$\left.\begin{aligned}&\Omega_1=\sqrt{\frac{U_o}{L_1\nu_1}}y,\qquad \Psi(\Omega_1)=\sqrt{\frac{\nu_1U_ox^2}{L_1}}G(\Omega_1),\\&u(\Omega_1)=\frac{U_ox}{L_1}G'(\Omega_1),\ \ v(\Omega_1)=\sqrt{\frac{\nu_1U_o}{L_1}}G(\Omega_1),\\&\Theta(\Omega_1)=\frac{T-T_\infty}{T_w-T_o},\qquad \Upsilon(\Omega_1)=\frac{C-C_\infty}{C_w-C_o},\end{aligned}\right\} \tag{13}$$

Introducing Eq. (13) into Eqs. (2), (7), and (8), we get the following set of ordinary differential equations (Eqs. (14), (15), and (16))

$$\left.\begin{aligned} &G''' - G'^2 + GG'' + \alpha_1\left(G''^2 - 2G'G''' + GG^4\right) \\ &+\lambda_1\left[\left(1+\widehat{\beta}_t\Theta\right)\Theta + \widehat{N}_1\left(1+\widehat{\beta}_c\Upsilon\right)\Upsilon\right] = 0, \end{aligned}\right\} \tag{14}$$

$$\left.\begin{aligned} &\Theta'' + Pr\left(G\Theta' + \widehat{N}_b\Upsilon'\Theta' + \widehat{N}_t\Theta'^2 - (\Theta+P_1)G'\right) + \left(B_1G' + B_2\right) \\ &-Pr\delta_2\left(G^2\Theta'' + \left(G'^2 - GG''\right)(\Theta+P_1) - GG'\Theta'\right) = 0, \end{aligned}\right\} \tag{15}$$

$$\left.\begin{aligned} &\Upsilon'' + ScG\Upsilon' + \frac{\widehat{N}_t}{\widehat{N}_b}\Theta'' - \delta_3 Sc\left(G^2\Upsilon'' + \left(G'^2 - GG''\right)(\Upsilon+P_2) - GG'\Upsilon'\right) \\ &-Sc\left(\gamma_1\Upsilon + (\Upsilon+P_2)G' + \xi_1(1+\delta\Theta)^n exp\left[-\frac{A_1}{1+\delta\Theta}\right]\right) = 0, \end{aligned}\right\} \tag{16}$$

Transformed boundary conditions (Eq. (17)) are

$$\left.\begin{aligned} &\mathrm{G}'(0) = 1,\ \ \mathrm{G}(0) = V_s,\ \ \Theta(0) = 1 - \mathrm{P}_1,\ \ \Upsilon(0) = 1 - \mathrm{P}_2, \\ &\lim_{\Omega_1\to\infty}\mathrm{G}' = 0,\ \ \lim_{\Omega_1\to\infty}\Theta = 0,\ \ \lim_{\Omega_1\to\infty}\Upsilon = 0, \end{aligned}\right\} \tag{17}$$

Mathematically, the non-dimensional governing parameters are defined as follows

$\alpha_1 = \frac{\Lambda_1}{\nu_1 L_1}$	Signifies for viscoelastic factor
$\gamma_1 = \frac{\widehat{k}_2 L_1}{U_o}$	Chemical reaction parameter
$\delta = \frac{T_w - T_o}{T_\infty}$	Temperature difference
$\delta_2 = \frac{\widehat{\Gamma}_e U_o}{L_1}$	Thermal relaxation time
$\delta_3 = \frac{\widehat{\Gamma}_c U_o}{L_1}$	Solutal relaxation time,
$A_1 = \frac{E_2^*}{T_\infty k}$	Activation energy
$\xi_1 = \frac{K_r^{*2} L_1}{U_o}$	Reaction rate constant
$Sc = \frac{\nu_1}{D_B}$	Schmidt number
$P_1 = \frac{d_2}{d_1}$	Thermal stratification parameter
$P_2 = \frac{d_4}{d_3}$	Solutal stratification parameter
$\lambda_1 = \frac{L_1^2(T_w - T_o)\widehat{g}_2\Gamma_1}{U_o^2 x^2}$	Mixed convection parameter
$\widehat{N}_t = \frac{\tau_1 \mathrm{D}_T(T_w - T_o)}{T_\infty \nu_1}$	Thermophorsis parameter
$\widehat{\beta}_t = \frac{\Gamma_2(T_w - T_o)}{\Gamma_1}$	Nonlinear thermal mixed convection parameter
$\widehat{\beta}_c = \frac{\Gamma_4(\mathrm{C}_w - \mathrm{C}_o)}{\Gamma_3}$	Nonlinear solutal mixed convection parameter
$\widehat{N}_1 = \frac{\Gamma_3(\mathrm{C}_w - \mathrm{C}_o)}{\Gamma_1(T_w - T_o)}$	Concentration to thermal bouncy ratios

The skin friction coefficient (C_G), local Nusselt (Nu_x) and Sherwood (Sh_x) numbers take the form Eq (18)

$$C_G = \frac{2\tau_w}{\rho U_w^2},\ \ Nu_x = \frac{xq_w}{k_f(T_w - T_o)},\ \ Sh_x = \frac{xj_w}{\mathrm{D}_B(\mathrm{C}_w - \mathrm{C}_o)}, \tag{18}$$

with wall shear stress (τ_w), wall heat and mass fluxes (q_w j_w) are given in Eqs. (19), (20), and (21)

$$\tau_w = \left|\nu\frac{\partial u}{\partial y} - \Lambda_1\left(u\frac{\partial^2 u}{\partial y \partial x} - 2\frac{\partial u}{\partial x}\frac{\partial u}{\partial y}\right)\right|_{y=0}, \tag{19}$$

$$q_w = -\left|k_f\frac{\partial T}{\partial y}\right|_{y=0}, \tag{20}$$

$$j_w = -\left|\mathrm{D}_B\frac{\partial C}{\partial y}\right|_{y=0}, \tag{21}$$

In dimensionless form, skin friction coefficient (C_G), local Nusselt (Nu_x) and Sherwood (Sh_x) numbers are written in Eqs. (22), (23), and (24)

$$\frac{1}{2}C_G(Re_x)^{0.5} = (1+\alpha_1)G'(0)G''(0), \tag{22}$$

$$Nu_x(Re_x)^{0.5} = -\Theta'(0), \tag{23}$$

$$Sh_x(Re_x)^{0.5} = -\Upsilon'(0), \tag{24}$$

in which $Re_z\left(=\frac{U_o X^2}{\nu_1 L_1}\right)$ is the local Reynolds number.

3. Methodology

Initial approximations $(\mathrm{G}^\circ(\Omega_1), \Theta^\circ(\Omega_1), \Upsilon^\circ(\Omega_1))$ and linear operators $(\widehat{\pounds}_\mathrm{G}, \widehat{\pounds}_\Theta, \widehat{\pounds}_\Upsilon)$ are mentioned in Eqs. (25) and (26).

$$\left.\begin{aligned} &\mathrm{G}^\circ(\Omega_1) = 1 + V_s - \exp(-\Omega_1), \\ &\Theta^\circ(\Omega_1) = (1 - \mathrm{P}_1)\exp(-\Omega_1), \\ &\Upsilon^\circ(\Omega_1) = (1 - \mathrm{P}_2)\exp(-\Omega_1), \end{aligned}\right\} \tag{25}$$

$$\widehat{\pounds}_\mathrm{G}[\mathrm{G}] = \mathrm{G}''' - \mathrm{G}',\ \ \widehat{\pounds}_\Theta[\Theta] = \Theta'' - \Theta,\ \ \widehat{\pounds}_\Upsilon[\Upsilon] = \Upsilon'' - \Upsilon, \tag{26}$$

with the following properties (Eq. (27))

$$\left.\begin{aligned} &\widehat{\pounds}_\mathrm{G}[\mathrm{c}_2\exp(-\Omega_1) + \mathrm{c}_1 + \mathrm{c}_3\exp(\Omega_1)] = 0, \\ &\widehat{\pounds}_\Theta[\mathrm{c}_4\exp(-\Omega_1) + \mathrm{c}_5\exp(\Omega_1)] = 0, \\ &\widehat{\pounds}_\Upsilon[\mathrm{c}_6\exp(-\Omega_1) + \mathrm{c}_7\exp(\Omega_1)] = 0. \end{aligned}\right\} \tag{27}$$

According to procedure (see Ref. [38]), we have (Eq. (28))

$$\left.\begin{aligned} &\mathrm{G}_\mathrm{m}(\Omega_1) = \mathrm{G}_\mathrm{m}^*(\Omega_1) + \mathrm{c}_2\exp(-\Omega_1) + \mathrm{c}_1 + \mathrm{c}_3\exp(\Omega_1), \\ &\Theta_\mathrm{m}(\Omega_1) = \Theta_\mathrm{m}^*(\Omega_1) + \mathrm{c}_4\exp(-\Omega_1) + \mathrm{c}_5\exp(\Omega_1), \\ &\Upsilon_\mathrm{m}(\Omega_1) = \Upsilon_\mathrm{m}^*(\Omega_1) + \mathrm{c}_6\exp(-\Omega_1) + \mathrm{c}_7\exp(\Omega_1). \end{aligned}\right\} \tag{28}$$

Where $(G_m^*(\Omega_1), \Theta_m^*(\Omega_1), \Upsilon_m^*(\Omega_1))$ are the special solutions and $\mathrm{c_j}(\mathrm{j} = 1-7)$ are the arbitrary constants defined in (Eq. (29))

$$\left.\begin{aligned} &c_1 = \left.\frac{\partial G_m^*}{\partial\Omega_1}\right|_{\Omega_1=0} - G_m^*(0),\ \ c_2 = \left.\frac{\partial G_m^*}{\partial\Omega_1}\right|_{\Omega_1=0},\ \ c_3 = 0, \\ &c_4 = -\Theta_m^*(\Omega_1)\big|_{\Omega_1=0},\ \ c_6 = -\Upsilon_m^*(\Omega_1)\big|_{\Omega_1=0},\ \ c_5 = c_7 = 0. \end{aligned}\right\} \tag{29}$$

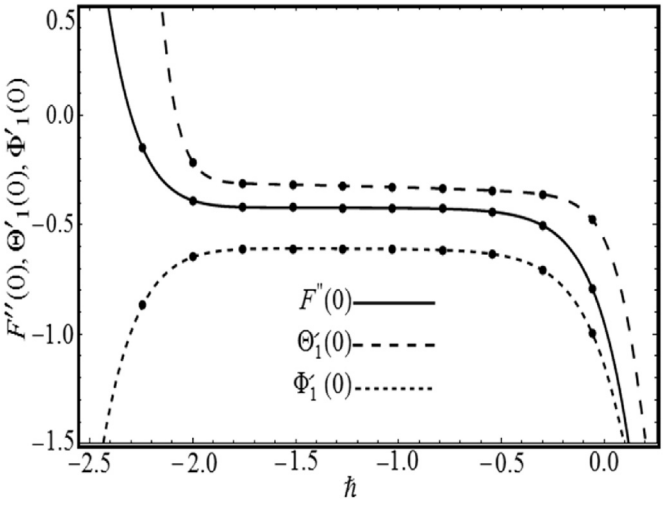

Fig. 2. h_F, h_{Θ_1} and h_{Φ_1} – *curves*.

4. Analysis

Here, we have employed Homotopy analysis method for our highly nonlinear problem to develop the convergence solutions. In 1992, Liao [37] initially established the concept of Homotopy technique. This method (HAM) is responsible to provide the guarantee of convergence of the approximation series. Here h − curves are sketched to see the appropriate ranges of h_G, h_Θ and h_Υ in Fig. 2. The admissible convergent regions parallel to h − axis are $(-1.0 \le h_G \le -0.5)$, $(-1.3 \le h_\Theta \le -0.5)$ and $(-1.4 \le h_\Upsilon \le -1.1)$, respectively. Convergence of velocity $G''(0)$, temperature $\Theta'(0)$ and concentration $\Upsilon'(0)$ is attained at 18^{th}, 26^{th} and 30^{th} order of approximation respectively (see Table 1).

5. Results & discussion

In this section we will discuss in detail the behavior of velocity $G'(\Omega_1)$, concentration $\Upsilon(\Omega_1)$, temperature $\Theta(\Omega_1)$, heat transfer rate and mass transfer Nusselt number for various flow variables in graphical and tabulated form. Fig. 3 presents the declining trend of $G'(\Omega_1)$ for greater $(\alpha_1 = 0.1, 0.3, 0.5, 0.7)$. Physically, higher (α_1) correspond to the enhancement in viscoelasticity through tensile stress. That develops resistance in boundary layer and hence velocity $G'(\Omega_1)$ profile declines. Fig. 4 elaborates behavior of (λ_1) for velocity $G'(\Omega_1)$ curve. Here $G'(\Omega_1)$ enriches for higher estimation of $(\lambda_1 = 0.1, 0.5, 1.0, 1.5)$. Since higher values of (λ_1) corresponds to the dominant role of thermal buoyancy force which helps to heighten the $G'(\Omega_1)$. Impact of $(\widehat{N}_b)$ and $(\widehat{N}_t)$on temperature $\Theta(\Omega_1)$ is presented in Figs. 5 and 6 respectively. Increase in temperature $\Theta(\Omega_1)$ and apposite boundary layer thickness is found for greater marks of $(\widehat{N}_b = 0.1, 0.5, 1.0, 1.5)$ (see Fig. 5). In fact, additional heat is generated due to random motion of liquid molecules within the frame of higher $(\widehat{N}_b)$. Hence, temperature $\Theta(\Omega_1)$ curve upsurges. Fig. 6 depicts same enhancing behaviour for fixed approximation of $(\widehat{N}_t)$ on $\Theta(\Omega_1)$. For higher approximation of $(\widehat{N}_t = 0.1, 0.5, 1.0, 1.5)$, fluid particles drag out from hotter region to colder region of medium. It is due to an increase in thermophoresis force that subsequently boosts up temperature $\Theta(\Omega_1)$ profile. Fig. 7 reveals the declining effect of temperature $\Theta(\Omega_1)$ for greater values of $(Pr = 0.1, 0.7, 1.5, 2.5)$. In fact, rise in (Pr) corresponds to weaker thermal diffusivity over the stronger momentum diffusivity due to which reduction in $\Theta(\Omega_1)$ is observed. Fig. 8 examines the declining trend of $\Theta(\Omega_1)$ for higher values of $(P_1 = 0.1, 0.3, 0.5, 0.7)$. In fact temperature difference $(T_w - T_\infty)$ gradually decreases for higher approximation of (P_1) that result in decrease of temperature. In Fig. 9 variation of $\Theta(\Omega_1)$ due to sundry values of (δ_2) is displayed. Here, both temperature and related boundary thickness are found to be decline in nature through greater value of $(\delta_2 = 0.1, 0.5, 1.0, 1.5)$. Physically, material particles require extra time for heat transfer to its neighboring particles due rise in thermal relaxation time. Fig. 10 reveals the impact of (B_1) on $\Theta(\Omega_1)$ profile. One can noticed that $\Theta(\Omega_1)$ is increasing function of $(B_1 = 0.1, 0.3, 0.5, 0.7)$. Scientifically, higher value of (B_1)

Table 1
Convergence analysis when $\gamma_1 = 0.8$, $\widehat{\beta}_t = \widehat{\beta}_c = \alpha_1 = B_1 = V_s = \delta_2 = 0.2$, $\widehat{N}_b = 0.5, \xi_1 = \widehat{N}_1 = A_1 = \delta = 1.0$, $B_2 = \delta_3 = P_1 = 0.3$, $Sc = 1.5$, $\widehat{N}_t = \lambda_1 = 0.5$, $P_2 = 0.1$, $Pr = 0.7$, $n = 0.5$.

Approximation Order	$-G''(0)$	$-\Theta'(0)$	$-\Upsilon'(0)$
1	0.6253	0.2014	2.4943
8	0.6545	0.2386	2.5761
12	0.7138	0.3495	2.6874
18	0.7957	0.3828	2.7136
26	0.7957	0.4395	2.7250
30	0.7957	0.4395	2.7544
36	0.7957	0.4395	2.7544
40	0.7957	0.4395	2.7544
42	0.7957	0.4395	2.7544

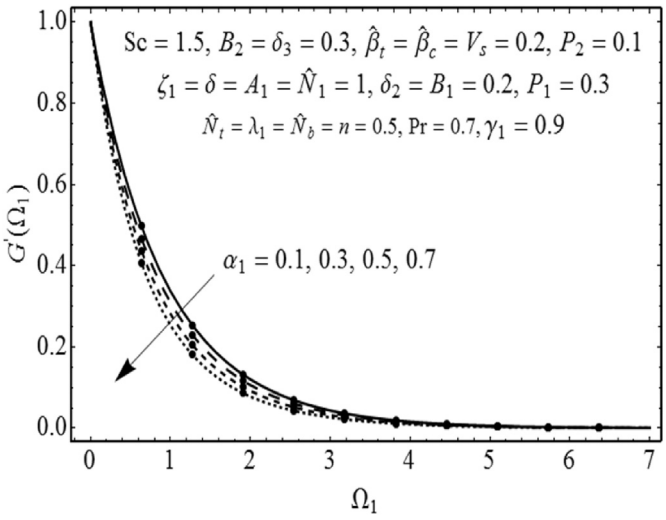

Fig. 3. Response of $G'(\Omega_1)$ *with* α_1.

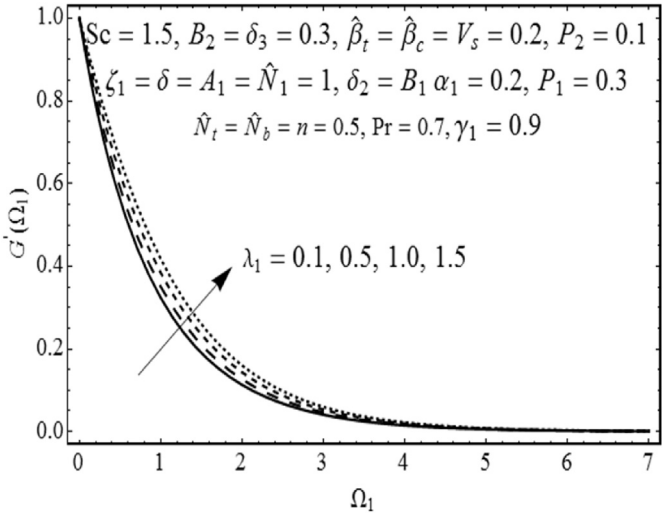

Fig. 4. Response of $G'(\Omega_1)$ *with* λ_1.

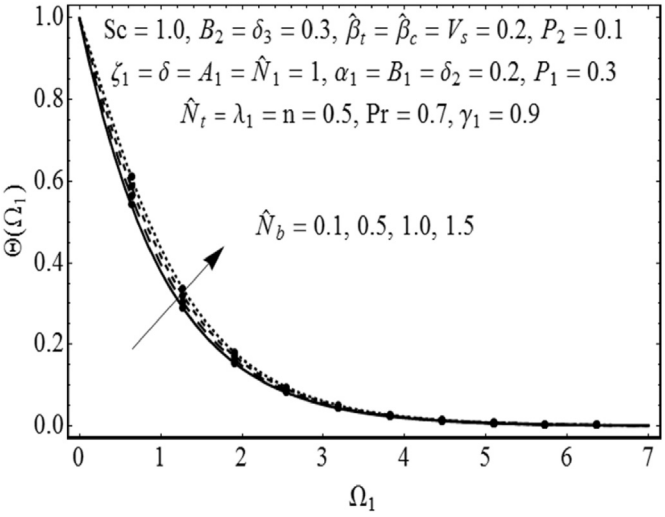

Fig. 5. Response of $\Theta(\Omega_1)$ with $\widehat{N}_b$.

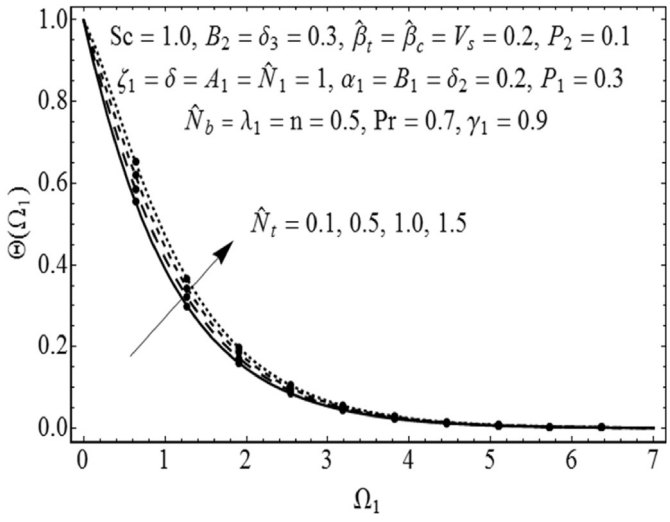

Fig. 6. Response of $\Theta(\Omega_1)$ *with* $\widehat{N}_t$.

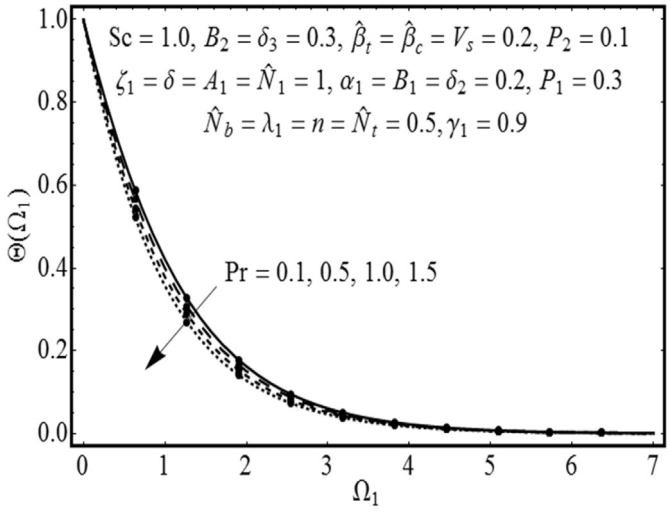

Fig. 7. Response of $\Theta(\Omega_1)$ *with Pr*.

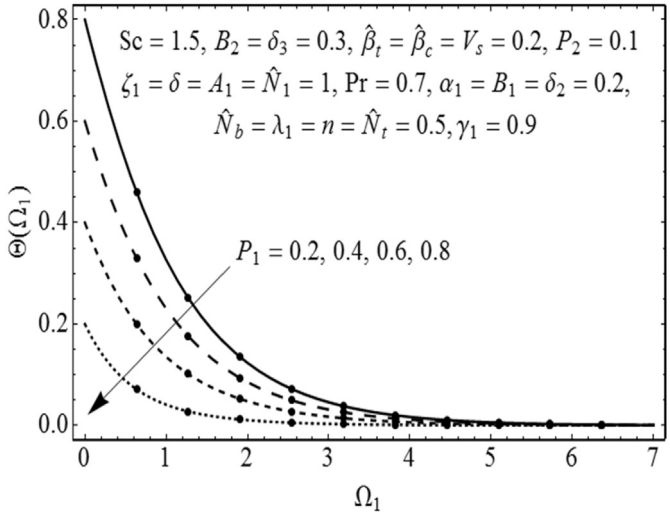

Fig. 8. Response of $\Theta(\Omega_1)$ *with* P_1.

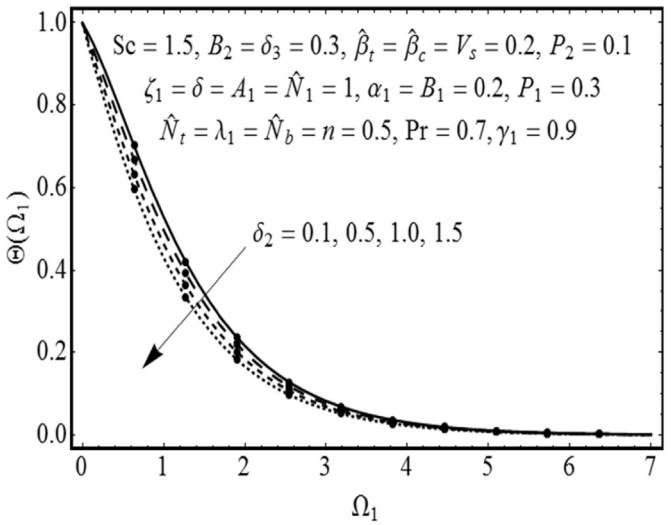

Fig. 9. Response of $\Theta(\Omega_1)$ *with* δ_2.

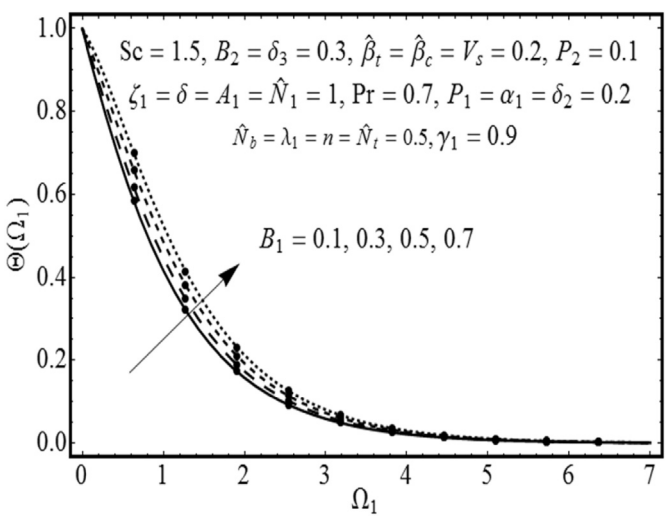

Fig. 10. Response of $\Theta(\Omega_1)$ *with* B_1.

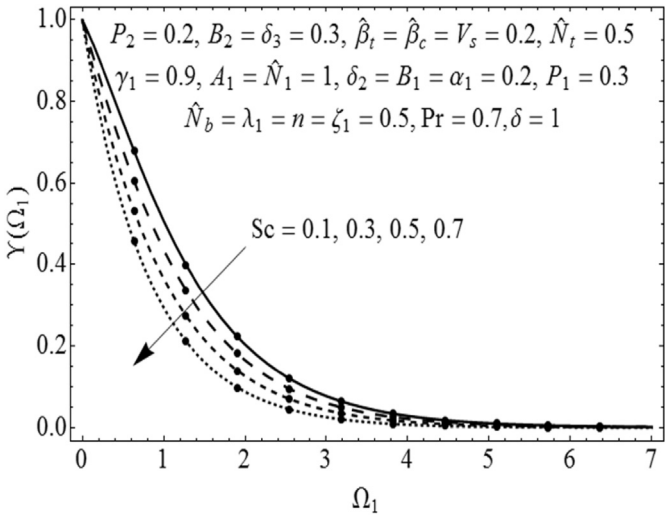

Fig. 11. Response of $\Upsilon(\Omega_1)$ with *Sc*.

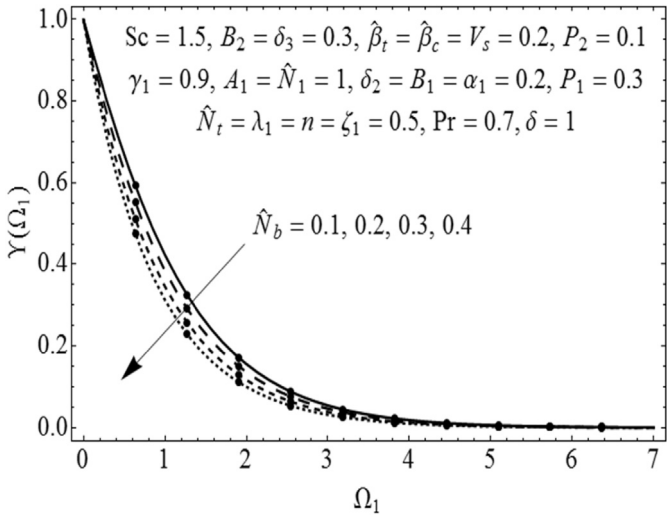

Fig. 12. Response of $\Upsilon(\Omega_1)$ with $\widehat{N}_b$.

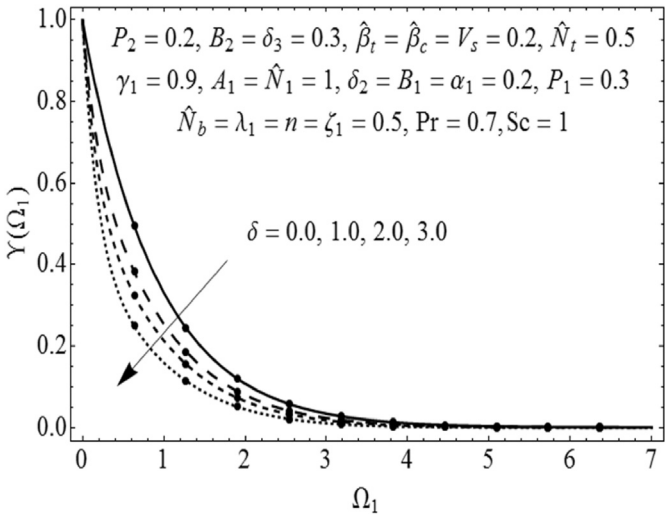

Fig. 14. Response of $\Upsilon(\Omega_1)$ with δ.

corresponds to increase in the thermal boundary layer thickness that performs as an agent to produce more heat. Due to this fact, an increase in $\Theta(\Omega_1)$ is observed for greater estimation of (B_1). Impact of (Sc) on $\Upsilon(\Omega_1)$ is deliberated in Fig. 11. Concentration outline reduces for larger values of $(Sc = 0.1, 0.3, 0.5, 0.7)$. Since higher values of (Sc) resembles to the lower mass diffusivity which reduces concentration $\Upsilon(\Omega_1)$ profile. Fig. 12 displays the role of $(\widehat{N}_b)$ on concentration $\Upsilon(\Omega_1)$. For higher values of $(\widehat{N}_b = 0.1, 0.2, 0.3, 0.4)$ the concentration $\Upsilon(\Omega_1)$ and boundary thickness have assertive behavior. This assertive response produces more collision among fluid particles due to which $\Upsilon(\Omega_1)$ diminishes. Fig. 13 elaborates the character of $(\widehat{N}_t)$ on $\Upsilon(\Omega_1)$. For greater estimation of $(\widehat{N}_t = 0.1, 0.2, 0.3, 0.4)$ fluid thermal conductivity develops promptly. Such extra thermal conductivity corresponds to rise in $\Upsilon(\Omega_1)$. Fig. 14 displays the variation of $\Upsilon(\Omega_1)$ due to temperature change parameter (δ). Here decline role of $\Upsilon(\Omega_1)$ is analyzed for greater value of $(\delta = 0.0, 1.0, 2.0, 3.0)$. Physically, it indicates that concentration boundary thickness $\Upsilon(\Omega_1)$ upsurges for higher temperature difference $(T_w - T_\infty)$. Fig. 15 is plotted to investigate $\Upsilon(\Omega_1)$ for different values of activation energy parameter (A_1). One can observed that increasing behavior of concentration $\Upsilon(\Omega_1)$ exists for higher marks of $(A_1 = 1.0, 2.0, 3.0, 5.0)$. Physically, greater (A_1) decreases the modified Arrhenius function which eventually endorses the generative chemical reaction. Therefore $\Upsilon(\Omega_1)$

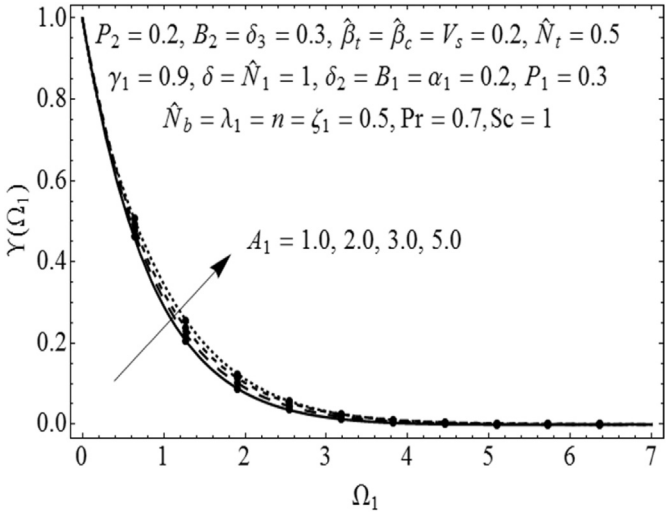

Fig. 15. Response of $\Upsilon(\Omega_1)$ with A_1.

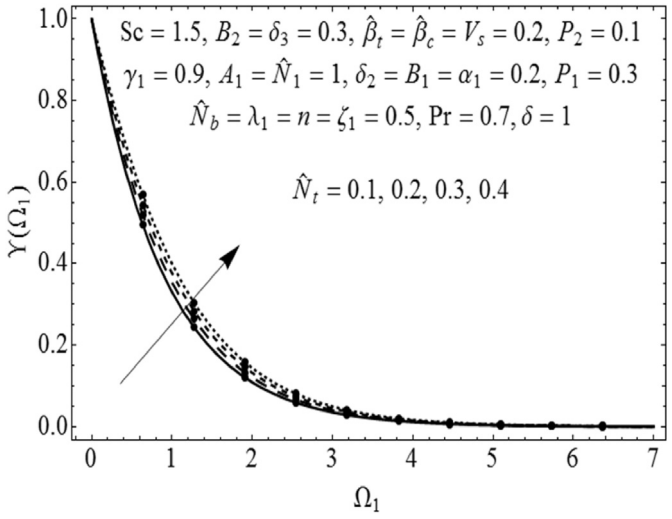

Fig. 13. Response of $\Upsilon(\Omega_1)$ with $\widehat{N}_t$.

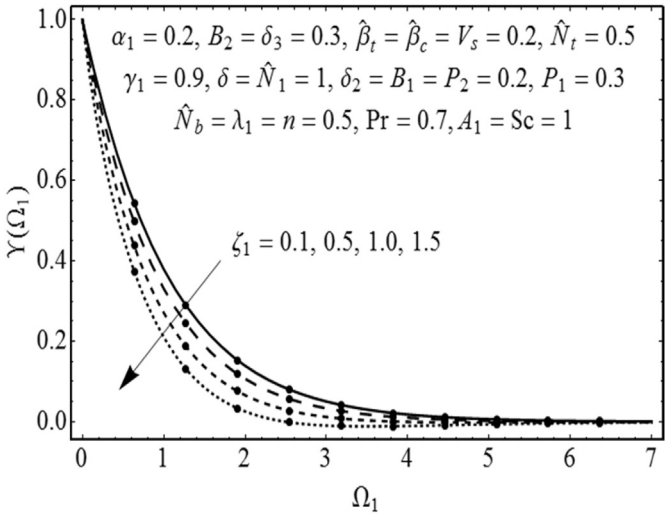

Fig. 16. Response of $\Upsilon(\Omega_1)$ with ξ_1.

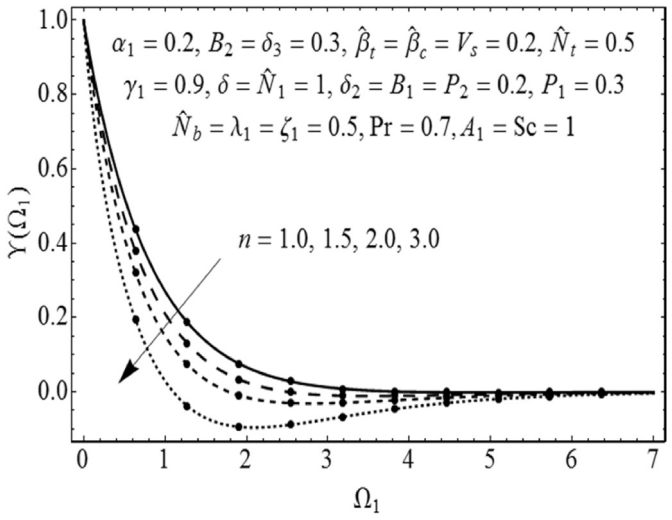

Fig. 17. Response of $\Upsilon(\Omega_1)$ with n.

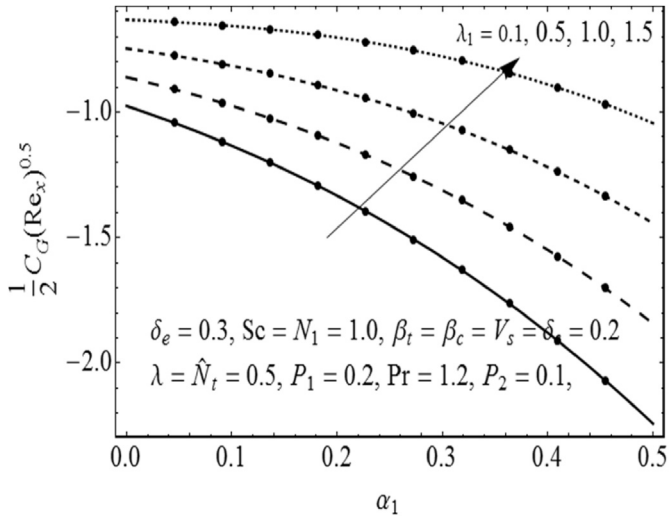

Fig. 19. Response of $\frac{1}{2}C_G(Re_x)^{0.5}$ with λ_1.

enriches. Higher variation of ($\xi_1 = 0.1, 0.5, 1.0, 1.5$) corresponds to increase in rate of destructive chemical reaction which terminates/dissolves the fluid specie more effectively (see Fig. 16). Hence, concentration $\Upsilon(\Omega_1)$ decays. Fig. 17 interprets the impact of fitted rate constant ($n = 1.0, 1.5, 2.0, 3.0$) on $\Upsilon(\Omega_1)$. Here $\Upsilon(\Omega_1)$ is found to be decreasing function of (n). The role of skin friction coefficient (C_G), Nusselt number (Nu_x) and Sherwood Number (Sh_x) for emerging parameters ($\hat{N}_b$), (B_2), (Pr), (ξ_1) and (λ_1) are presented in Figs. 18, 19, 20, 21, 22 and 23 respectively. It is depicted from Figs. 18 and 19 that skin friction coefficient (C_G) enhances for larger values of both parameters ($\hat{N}_b = 0.1, 0.5, 1.0, 1.5$) and ($\lambda_1 = 0.1, 0.5, 1.0, 1.5$), respectively. While behavior of Nusselt number $Nu_x(Re_x)^{0.5}$ for (B_2) and (Pr) are perceived in Figs. 20 and 21. Fig. 20 depicts the decline role of Nu_x for greater marks of ($B_2 = 0.1, 0.3, 0.5, 0.7$). Whereas reverse impact is identified for fixed ($\Pr = 0.1, 0.5, 1.0, 1.5$) (see Fig. 22). Impact of local Sherwood number $Sh_x(Re_x)^{0.5}$ for (ζ_1) and (λ_1) are displayed in Figs. 22 and 23. Here we revealed that $Sh_x(Re_x)^{0.5}$ enhances via ($\zeta_1 = 0.1, 0.5, 1.0, 1.5$) and it diminishes for fixed values of ($\lambda_1 = 0.1, 0.5, 1.0, 1.5$).

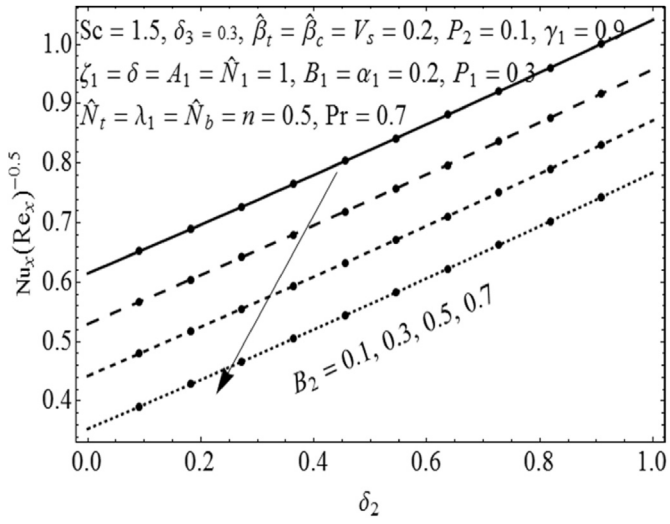

Fig. 20. Response of $Nu_x(Re_x)^{-0.5}$ with B_2.

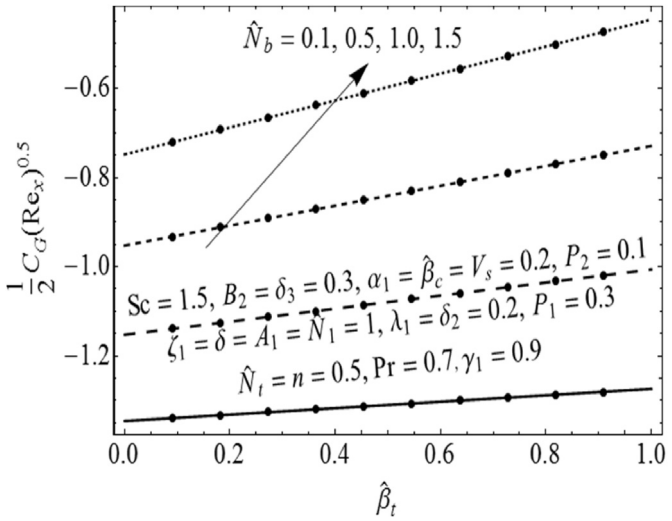

Fig. 18. Response of $\frac{1}{2}C_G(Re_x)^{0.5}$ with $\hat{N}_b$.

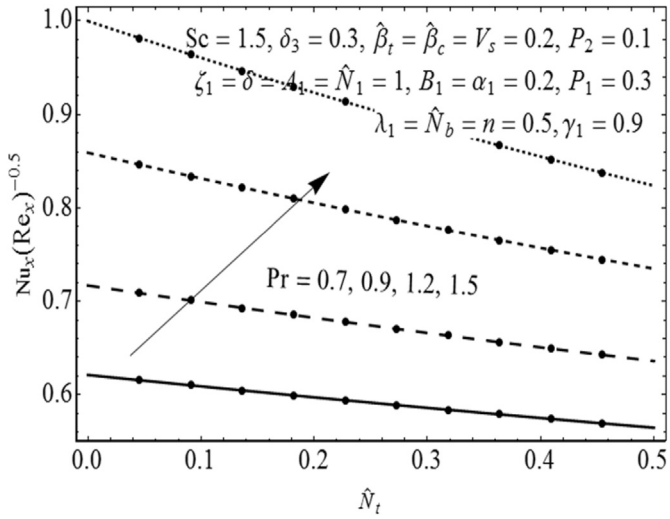

Fig. 21. Response of $Nu_x(Re_x)^{-0.5}$ with Pr.

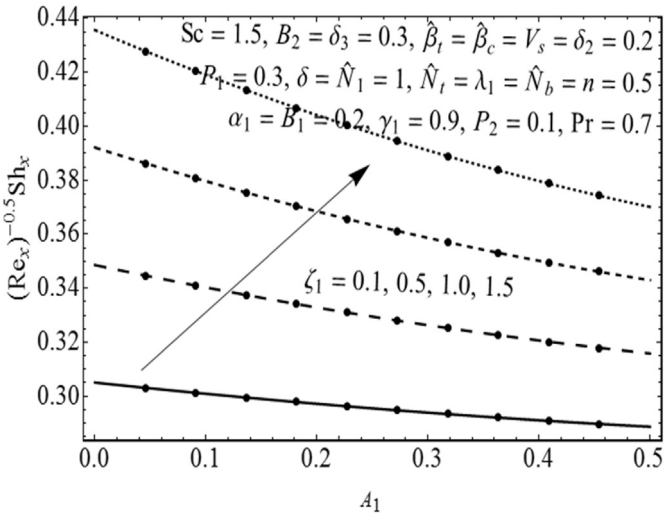

Fig. 22. Response of $Sh_x(Re_x)^{-0.5}$ with ξ_1.

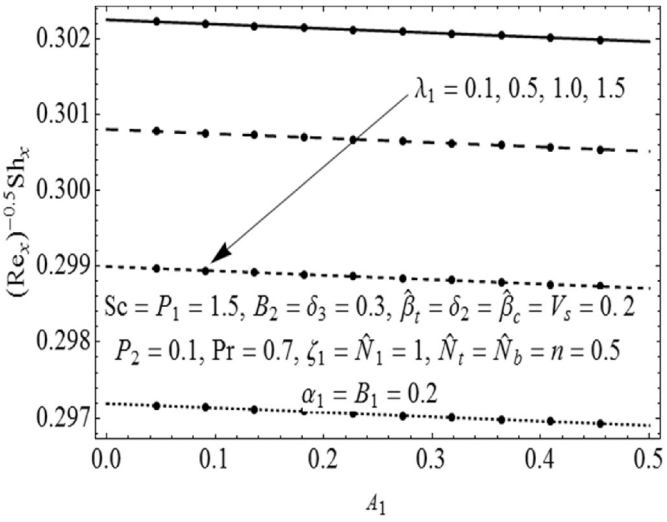

Fig. 23. Response of $Sh_x(Re_x)^{-0.5}$ with λ_1.

6. Conclusions

The present communication provides the homotopic solution of nonlinear convective flow of Walter-B nanofluid with non-uniform heat generation/absorption, nonlinear mixed convection, thermal and solutal stratification, binary chemical reaction and activation energy. Heat and mass transfer analysis has been performed with Cattaneo-Christov double-diffusion model. Main findings of the study are listed below:

- Velocity profile $G'(\Omega_1)$ declines for higher values of viscoelastic factor (α_1) while it upsurge for larger marks of mixed convection parameter (λ_1).
- Temperature field $\Theta(\Omega_1)$ enhances for greater values of flow parameters $(\widehat{N}_b)$, $(\widehat{N}_t)$ and (B_1).
- Both temperature and concentration distributions decline for greater thermal and solutal relaxation parameters, respectively.
- For greater estimations of activation energy parameter (A_1) concentration profile $\Upsilon(\Omega_1)$ enhances while reverse impact is noticed for reaction rate constant (ζ_1).
- Reverse behavior of concentration (Ω_1) field is pronounced in view of $(\widehat{N}_b)$ and $(\widehat{N}_t)$.
- Skin friction coefficient is amplified via Brownian parameter $(\widehat{N}_b)$.

Declarations

Author contribution statement

Misbah Ijaz: Conceived and designed the analysis; Analyzed and interpreted the data; Wrote the paper.

Muhammad Ayub: Conceived and designed the analysis; Analyzed and interpreted the data; Contributed analysis tools or data.

Funding statement

This research did not receive any specific grant from funding agencies in the public, commercial, or not-for-profit sectors.

Competing interest statement

The authors declare no conflict of interest.

Additional information

No additional information is available for this paper.

References

[1] L. Zheng, L. Wang, X. Zhang, Analysis solutions of unsteady flow and heat transfer on a permeable stretching sheet with non-uniform heat source/sink, Commun. Nonlinear Sci. Numer. Simul. 16 (2011) 731–740.
[2] X. Su, L. Zheng, X. Zhang, J. Zhang, MHD mixed convective heat transfer over a permeable stretching wedge with thermal radiation and ohmic heating, Chem. Eng. Sci. 78 (2012) 1–8.
[3] J. Sui, L. Zheng, X. Zhang, G. Chen, Mixed convection heat transfer in power law fluids over a moving conveyor along an inclined plate, Int. J. Heat Mass Transf. 85 (2015) 1023–1033.
[4] S. Han, L. Zheng, C. Li, X. Zhang, Coupled flow and heat transfer in viscoelastic fluid with Cattaneo-Christov heat flux model, Appl. Math. Lett. 38 (2014) 87–93.
[5] J.B.J. Fourier, Théorie Analytique De La Chaleur, Paris, 1822.
[6] R. Fick, Medizinische Physik, 1856.
[7] C. Cattaneo, Some aspects of diffusion theory, Atti Semin. Mat Fis Univ. Modena Reggio Emilia 3 (1948) 83–101.
[8] F. Franchi, B. Straughan, Thermal convection at low temperature, J. Non-Equilibr. Thermodyn. 19 (1994) 368–374.
[9] P. Puri, P.K. Kythe, Discontinuities in velocity gradients and temperature in the Stoke's first problem with nonclassical heat conduction, Q. Appl. Math. 55 (1997) 167–176.
[10] C.I. Christov, On frame indifferent formulation of the Maxwell-Cattaneo model of finite-speed heat conduction, Mech. Res. Commun. 39 (2009) 481–486.
[11] J.A. Khan, M. Mustafa, T. Hayat, A. Alsaedi, Numerical study of Cattaneo-Christov heat flux model for viscoelastic flow due to an exponentially stretching surface, PLoS One 10 (2015), e0137363.
[12] M. Ijaz, M. Ayub, Nonlinear convective stratified flow of Maxwell nanofluid with activation energy, Heliyon 5 (2019).
[13] N. Muhammad, S. Nadeem, T. Mustafa, Squeezed flow of a nanofluid with Cattaneo-Christov heat and mass fluxes, Results Phys 7 (2017) 862–869.
[14] T. Hayat, T. Muhammad, A. Alsaedi, B. Ahmad, Three-dimensional flow of nanofluid with Cattaneo-Christov double diffusion, Results Phys 6 (2016) 897–903.
[15] J. Sui, L. Zheng, X. Zhang, Boundary layer heat and mass transfer with Cattaneo-Christov double-diffusion in upper-convected Maxwell nanofluid past a stretching sheet with slip velocity, Int. J. Therm. Sci. 104 (2016) 461–468.
[16] W.A. Khan, M. Khan, A.S. Alshomrani, Impact of chemical processes on 3D Burgers fluid utilizing Cattaneo-Christov double-diffusion: applications of non-Fourier's heat and non-Fick's mass flux models, J. Mol. Liq. 223 (2016) 1039–1047.
[17] T. Hayat, A. Aziz, T. Muhammad, A. Alsaedi, Model and comparative study for flow of viscoelastic nanofluids with Cattaneo-Christov double diffusion, PLoS One 12 (2017), e0168824.
[18] M. Saquib, F. Ali, I. Khan, N.A. Sheikh, A. Khan, Entropy generation in different types of fractionalized nanofluids, Arabian J. Sci. Eng. 44 (2019) 531–540.
[19] R. Ravindran, N. Samyuktha, Unsteady mixed convection flow over stretching sheet in presence of chemical reaction and heat generation or absorption with non-uniform slot suction or injection, Appl. Math. Mech. 36 (2010) 1253–1272.
[20] M.K. Nayak, G.C. Dash, L.P. Singh, Heat and mass transfer effects on MHD viscoelastic fluid over a stretching sheet through porous medium in presence of chemical reaction, Propul. Power Research 5 (1) (2016) 70–80.
[21] B. Mallikarjuna, A.M. Rashad, A.J. Chamkha, S.H. Raju, Chemical reaction effects on MHD convective heat and mass transfer flow past a rotating vertical cone embedded in a variable porosity regime, Afr. Mat. 27 (2015) 645–665.
[22] T. Hayat, M. Mustafa, S. Asghar, Unsteady flow with heat and mass transfer of a third grade fluid over a stretching surface in the presence of chemical reaction, Nonlinear Anal. R. World Appl. 11 (2010) 3186–3197.

[23] M. Zubair, M. Ijaz, T. Abbas, A. Riaz, Analysis of modified Fourier law in flow of ferromagnetic Powell-Eyring fluid considering two equal magnetic dipoles, Can. J. Phys. (2018).
[24] F.M. Abbasi, S.A. Shehzad, T. Hayat, B. Ahmad, Doubly stratified mixed convection flow of maxwell nanofluid with heat generation/absorption, J. Magn. Magn. Mater. 404 (2016) 159–165.
[25] M. Ijaz, M. Ayub, M. Zubair, A. Riaz, On stratified flow of ferromagnetic nanofluid with heat generation/absorption, Phys. Scripta 94 (4) (2019).
[26] T. Hayat, M. Waqas, M.I. Khan, A. Alsaedi, Analysis of thixotropic nanomaterial in a doubly stratified medium considering magnetic field effects, Int. J. Heat Mass Transf. 102 (2016) 1123–1129.
[27] T. Hayat, M. Imtiaz, A. Alsaedi, Unsteady flow of nanofluid with double stratification and magnetohydrodynamics, Int. J. Heat Mass Transf. 92 (2016) 100–109.
[28] F.M. Abbasi, S.A. Shehzad, T. Hayat, M.S. Aluuthali, Mixed convection flow of jeffrey nanofluid with thermal radiation and double stratification, J. Hydrodyn Ser-B 28 (2016) 840–849.
[29] T. Hayat, Z. Hussain, A. Alsaedi, Influence of heterogeneous-homogeneous reactions in thermally stratified stagnation point flow of an oldroyd-B fluid, Results Phys 6 (2016) 1161–1167.
[30] J. Buongiorno, Convective transport in nanofluids, ASME-J. Heat Transf. 128 (2006) 240–250.
[31] R.K. Tiwari, M.K. Das, Heat transfer augmentation in a two-sided lid driven differentially heated cavity utilizing nanofluids, Int. J. Heat Mass Transf. 50 (2007) 2002–2018.
[32] A.V. Kuznetsov, D.A. Nield, Natural convective boundary-layer flow of a nanofluid past a vertical plate, Int. J. Therm. Sci. 49 (2010) 243–247.
[33] M. Ijaz, M. Ayub, Simulation of magnetic dipole and dual stratification in radiative flow of ferromagnetic Maxwell fluid, Heliyon 5 (2019), e01465.
[34] M.M. Bhatti, M.M. Rashid, Effects of thermo-diffusion and thermal radiation on Williamson nanofluid over a porous shrinking/stretching sheet, J. Mol. Liq. 221 (2016) 567–573.
[35] W.D. Beard, K. Walters, Elasto-viscous boundary layer flow, Proc. Camb. Phil. Soc. 60 (1964) 667.
[36] F. Ali, M. Saquib, I. Khan, N.A. Sheikh, Application of Caputo-Fabrizio derivatives to MHD free convection flow of generalized Walters'-B fluid model, Eur. Phys. J. Plus 131 (2016).
[37] S.J. Liao, The proposed Homotopy analysis technique for the solution of nonlinear problems, Ph.D. Thesis, Shanghai Jiao Tong Uni, 1992.
[38] T. Hayat, M. Ijaz, S. Qayyum, M. Ayub, A. Alsaedi, Mixed convective stagnation point flow of nanofluid with Darcy-Fochheimer relation and partial slip, Results Phys 9 (2018) 771–778.
[39] M. Saquib, I. Khan, S. Shafie, Natural convection channel flow of CMC-based CNTs nanofluid, Eur. Phys. J. Plus 133 (2018) 549.
[40] S. Ahmad, M. Yousaf, A. Khan, G. Zaman, Magnetohydrodynamic Fluid Flow and Heat Transfer over a Shrinking Sheet under the Influence of thermal Slip, Heliyon 4 (2018).
[41] K. Mehmood, S. Hussain, M. Sagheer, Mixed convection flow with non-uniform heat source/sink in a doubly stratified magnetonanofluid, AIP Adv. 6 (2016), 065126.